Current Steering in Retinal Stimulation via a Quasimonopolar Stimulation Paradigm

Paul B. Matteucci,[1] Spencer C. Chen,[2] David Tsai,[1,3,4] Christopher W. D. Dodds,[1] Socrates Dokos,[1] John W. Morley,[5,6] Nigel H. Lovell,[1] and Gregg J. Suaning[1]

[1]Graduate School of Biomedical Engineering, The University of New South Wales, Kensington, Australia
[2]School of Medical Sciences and Bosch Institute, The University of Sydney, Sydney, Australia
[3]Howard Hughes Medical Institute, Biological Sciences, Columbia University, New York, New York
[4]Bioelectronic Systems Lab, Electrical Engineering, Columbia University, New York, New York
[5]School of Medicine, The University of Western Sydney, Sydney, Australia
[6]School of Medical Sciences, The University of New South Wales, Kensington, Australia

Correspondence: Paul B. Matteucci, Graduate School of Biomedical Engineering, Level 5 Samuels Building, The University of New South Wales, NSW 2052, Australia; p.matteucci@unsw.edu.au.

Submitted: January 13, 2013
Accepted: April 29, 2013

Citation: Matteucci PB, Chen SC, Tsai D, et al. Current steering in retinal stimulation via a quasimonopolar stimulation paradigm. *Invest Ophthalmol Vis Sci*. 2013;54:4307–4320. DOI:10.1167/iovs.13-11653

Purpose. Research to restore some degree of vision to patients suffering from retinal degeneration is becoming increasingly more promising. Several groups have chosen electrical stimulation of the remaining network of a degenerate retina as a means to generate discrete light percepts (phosphenes). Approaches vary significantly, with the greatest difference being the location of the stimulating electrode itself.

Methods. Suprachoroidal positioning offers excellent mechanical stability and surgical simplicity; however, at the cost of activation thresholds and focused stimulation due to the distance from the electrodes to the target neurons. Past studies proposed a hexapolar electrode configuration to focus the cortical activation and minimize cross-talk between electrodes during concurrent stimulation. The high impedance nature of the choroid and pigment epithelium, however, cause current to shunt between the stimulating and return electrodes, resulting in even higher activation thresholds. In our study, we analyzed the effect of stimulating the feline retina using a quasimonopolar stimulation by simultaneously stimulating a hexapolar and distant monopolar return configurations.

Results. Results of in vivo studies showed that quasimonopolar stimulation can be used to maintain the activation containment properties of hexapolar stimulation, while lowering the activation threshold to values almost equivalent to those of monopolar stimulation.

Conclusions. The optimal stimulus was found to be composed of a subthreshold monopolar stimulus combined with a suprathreshold hexapolar stimulation. This resulted in a decrease of activation threshold of 60% with respect to hexapolar alone, but with no discernible deleterious effect on the charge containment of a pure hexapolar stimulation.

Keywords: suprachoroidal, vision prosthesis, current steering, stimulation

Electrical stimulation has been used effectively for decades to treat and survive debilitating diseases and conditions.[1–3] Building on the understanding and knowledge gained from pacemakers, deep brain stimulators, and cochlear implants, the attention of various research groups has now been drawn to those conditions that deprive humans of what is arguably the most relied upon sense, vision. Initial attempts to elicit visual sensations date back as far as 1755, when Charles LeRoy elicited percepts of light in a patient using an electrical charge.[4] Since these humble beginnings, methods and materials have made significant progress, leading to the pursuit of multiple paths. As with most systems, the perfect device remains elusive, and various solutions have been proposed targeting the visual cortex,[5–9] lateral geniculate nucleus, and optic nerve.[10,11] In recent years, approaches at the center of intense research have focused on electrical stimulation of retinal neurons that survive neural degenerative diseases.[12–14] Even within the retinal stimulating prosthesis field, there are various approaches and ideas regarding the optimal location of the electrodes used to stimulate the tissue. Stimulating electrodes have been positioned on the retina (epiretinal), below the retina (subretinal), between the choroid and sclera (suprachoroidal), and outside the sclera (episcleral).[15] The epiretinal approach[16–18] involves positioning the stimulating electrodes directly adjacent to the retinal ganglion cells and nerve fiber layer that ultimately forms the optic nerve. This allows the electrodes to be in close proximity to the ganglion cells, with results showing that this position yields the lowest activation threshold of all the approaches.[19] However, mechanical stability and fixation of the electrode can prove difficult.[20,21] The subretinal approach improves the mechanical stability; however, it involves complex surgery to detach the retina partially from the pigment epithelium at the implantation site.[22]

From these potential limitations, the suprachoroidal approach[23–25] was developed, allowing the electrode array to be inserted and positioned with a simple scleral incision.[26] The suprachoroidal space positions the electrode between two mechanically robust layers of the retina (choroid and sclera), and is unlikely to cause fibrosis of the pigment epithelium. However, increased distance from the target cells has a

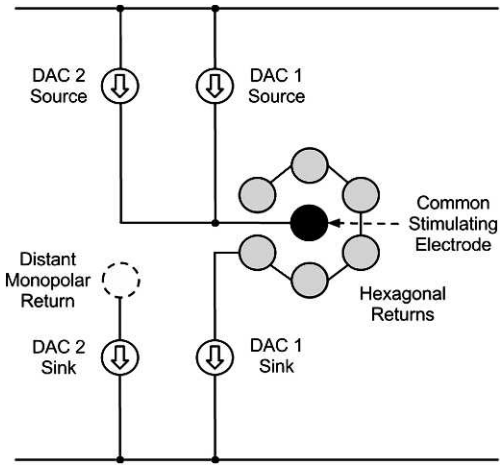

Figure 1. Quasimonopolar stimulation schematic. Two sources of the stimulator's constant-current DACs are connected to the same stimulating electrode (*black*), with the return paths of DAC1 going to the surrounding electrodes and the return of DAC2 going to a distant monopolar return.

detrimental effect on stimulation charge containment, thus reducing the efficacy of discrete phosphene formation.

Most early suprachoroidal studies have focused primarily on monopolar stimulation, with the return electrode either in the vitreous or on the sclera.[23,25,27] With the increase in electrode numbers and density, the complex electric field interactions between stimulation electrodes will affect the ability to elicit discrete phosphenes using monopolar stimulation.[28–30] An alternative electrode configuration was proposed. This configuration couples each stimulating electrode with six surrounding electrodes (Fig. 1) that act as guards (hexapolar) to contain and localize the charge. This proved effective at charge containment and confirmed findings from studies in auditory prosthetics have shown that using different return path configurations can result in greater spatial selectivity.[31–34] Thus, this strategy also may be beneficial for retinal implants.

Mathematical modeling of hexapolar stimulation, however, indicates that only a portion of the current injected from the suprachoroidal space permeates the target tissue, with large amounts being shunted laterally.[35] In vivo and in vitro studies have lent support to this hypothesis,[31,36] wherein an increase in hexapolar activation threshold is observed to be up to three times that of monopolar.

In our study, we proposed and characterized the effect of a new current steering strategy of a suprachoroidal retinal implant on elicited responses measured using a penetrating electrode array inserted in the primary visual cortex. We measured the effect of stimulating concurrently using a distant monopolar and hexapolar return configuration, in what we described as a quasimonopolar stimulation. We examined the effects of quasimonopolar stimulation on activation threshold thresholds and spatial localization. A new method was developed to analyze spatial localization using conditional probability to increase the accuracy of the results. Results showed that by using a subthreshold monopolar component, a quasimonopolar stimulation can achieve activation thresholds that approximate those of a monopolar stimulation, with minimal effect of the charge localization of hexapolar stimulation.

Materials and Methods

Retinal Stimulating Array

A 24-electrode stimulating array was developed and fabricated in the authors' laboratory in accordance with the processes described previously[37] (Fig. 2). Briefly, electrodes were fabricated by laser micro machining a platinum (Pt) foil on a polydimethylsiloxane (PDMS) substrate, with the addition of a layer of polyethylene terephthalate for mechanical strength. This resulted in an overall electrode thickness of approximately 600 μm. Individual electrode diameters were 380 μm and center-to-center distance was 730 μm. Electrodes were positioned in a hexagonal configuration, allowing 10 of the 24 stimulating electrodes to be surrounded by a full ring of return electrodes, and, thus, allowing the authors to use the hexapolar current-steering configuration.[31]

Quasimonopolar Retinal Stimulation

Figure 1 illustrates the electrical connection established between the two stimulators' digital to analog converters (DACs) and the electrodes on the stimulating array. The matching push-pull configuration of the current sources and sinks used in the stimulator results in an equal amount of

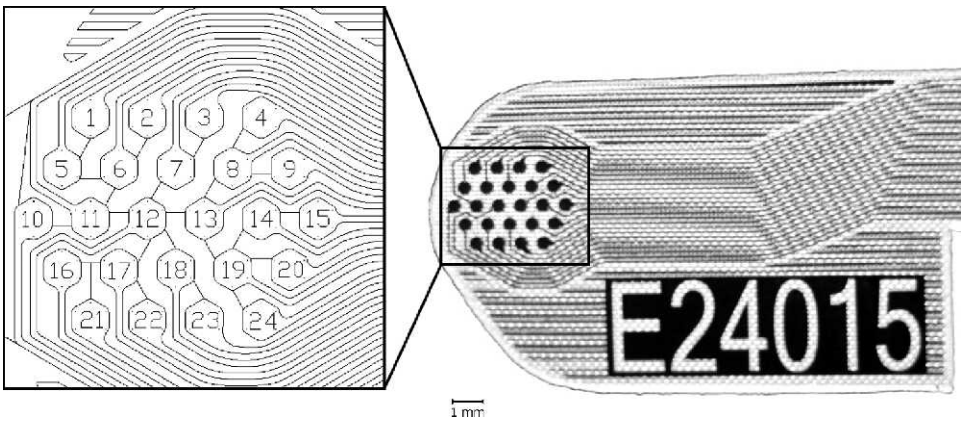

Figure 2. Photograph of actual 24-channel Pt electrode used in experiments (*right*) highlighting the number of each electrode (*left detail*). The electrodes are positioned to allow a hex guard configuration to improve charge containment. The form factor of the array is such that it is consistent with a planned 98-channel device undergoing development within the authors' labs.

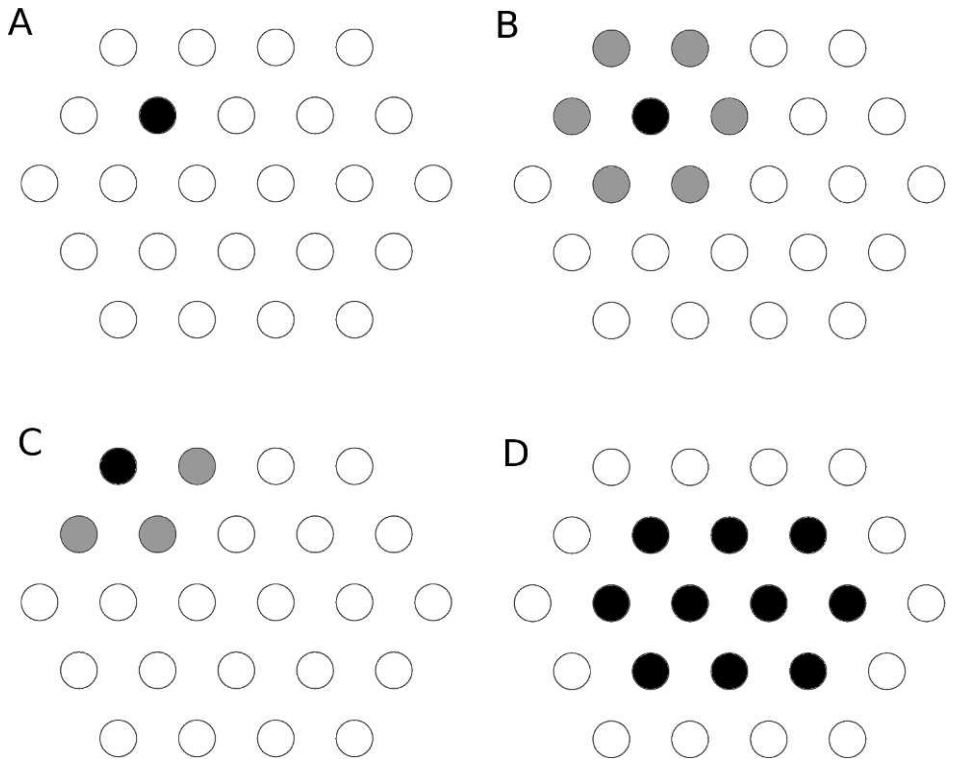

FIGURE 3. Quasimonopolar electrode availability. To achieve quasimonopolar stimulation, a monopolar (**A**) and hexapolar (**B**) configuration must be connected to the stimulator in parallel. Peripheral electrodes (**C**) do not allow a full ring of guard electrodes to be used, and partial and full hexapolar guards are significantly different at containing charge,[38] so only complete hexes were used. Consequently, the number of stimulating electrodes used in the study was confined to the central 10 electrodes (**D**). Stimulating electrodes are illustrated in *black* and return electrodes in *gray*.

current injected by the source of any one DAC being drawn by the matching sink for that DAC. During concurrent stimulation in which multiple DACs are active, this ensures that during the anodic phase, although multiple DACs are stimulating through the monopolar return, only the previously sourced amount of current is returned to the retinal electrodes. Two of the DACs of the stimulator were connected through the PXI switch matrix to the retinal stimulating array. Both sources of the two DACs were switched to connect to the same stimulating electrode; the sink of the first DAC then was connected to the distant monopolar return, while the sink of the second DAC was connected to the guard ring of electrodes surrounding the stimulating electrode (hexapolar). By injecting current using just one of the two DACs, pure monopolar or pure hexapolar stimulation could be investigated, while using both DACs simultaneously allowed us to characterize a combination of the two stimulation strategies.

The electrodes involved in the quasimonopolar stimulation are illustrated in Figure 3. Each of the 10 stimulating electrodes was selected in turn as the center of a hexagon and the stimulation conditions were randomized. Each condition initially was repeated 25 times (in the case of experiments 1 and 2), and increased to 50 for experiments 3, 4, and 5. To reduce the number of variables, all parameters of the stimulus conditions were fixed except for current amplitude. All stimuli were constant-current, charge-balanced, cathodic-first, with 500 μs per phase and a 10 μs interphase gap. Stimulations were performed every 888 ms. The stimulation current range was chosen to minimize the effects of exceeding charge injection limits in Pt defined by Rose and Robblee.[39] Every available permutation of monopolar and hexapolar injected currents was examined within the charge injection limit and the resolution of the stimulator, and are indicated in the Table.

Animal Preparation and Surgery

A series of in vivo experiments were conducted on normally sighted adult cats (Felis catus), with approval from the University of New South Wales (UNSW) Animal Care & Ethics Committee, and in adherence to the ARVO Statement for the Use of Animals in Ophthalmic and Vision Research.

Induction anesthesia was achieved with an intramuscular dose of ketamine (20 mg kg^{-1}) and xylazine (2.0 mg kg^{-1}). During surgical setup, intravenous and intraarterial catheters were inserted for administration of fluid and pharmacologic agents, and direct blood pressure measurement, respectively. Respiration rate, expired CO_2 level, and core temperature also were monitored by means of a tracheal tube and thermal probe. Anesthesia was maintained using a constant intravenous infusion of Alfaxan (1.1–1.3 mg kg^{-1}; Jurox Pty Ltd., Rutherford, New South Wales, Australia) delivered in 10 mL solution with 20 mL 5% glucose and 20 mL Hartmann's solution. Daily doses of dexamethasone (1.5 mg kg^{-1}) and broad-spectrum antibiotic (0.1 mL kg^{-1}) were administered intramuscularly, and atropine (0.2 mg kg^{-1}) was administered subcutaneously.

Positioning the electrode in the suprachoroidal space requires a simple surgical procedure that does not require a vitrectomy.[26] To facilitate insertion of the stimulating electrode array (Fig. 2) into the suprachoroidal space, a 9 mm incision was made 4 to 5 mm from the limbus and a pocket was created

TABLE. Combinations of Monopolar and Hexapolar Current Outputs Used During the Quasimonopolar Study

Hexapolar	Monopolar Current, μa									
Current, μA	0	36	72	107	142	180	215	257	327	363
0	x	x	x	x	x	x	x	x	x	x
36	x	x	x	x	x	x				
72	x	x	x	x	x	x				
107	x	x	x	x	x	x				
142	x	x	x	x	x	x				
180	x	x	x	x	x					
215	x	x	x	x	x					
257	x	x	x	x						
327	x	x	x	x						
363	x	x	x							
400	x	x	x							
436	x	x								
475	x	x								
512	x									
658	x									

to accommodate the electrode array using an inserter. The 24-channel stimulating electrode array was introduced and sutured into position to prevent movement during the experiment. Fundus imaging taken immediately following surgery shows the outline of the array and its position relative to the optic disk (Fig. 4). The animal then was moved to a stereotaxic frame for the remainder of the experiment.

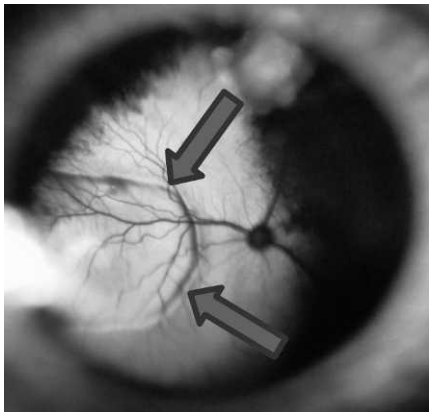

FIGURE 4. Fundus image of the cat retina with an implanted stimulating electrode array (highlighted by the *arrows*).

Atropine drops were administered on the eyes and contact lenses were placed to avoid corneal dehydration.

After the animal was moved to the stereotaxic frame, a craniotomy was performed[40] contralateral to the implanted eye, followed by a durotomy.

Mapping and Recording

The primary visual cortex was mapped using a ball electrode and a custom, 32-channel surface electrode (4 × 6 electrodes, 670 μm pitch) while stimulating the retina implant at a

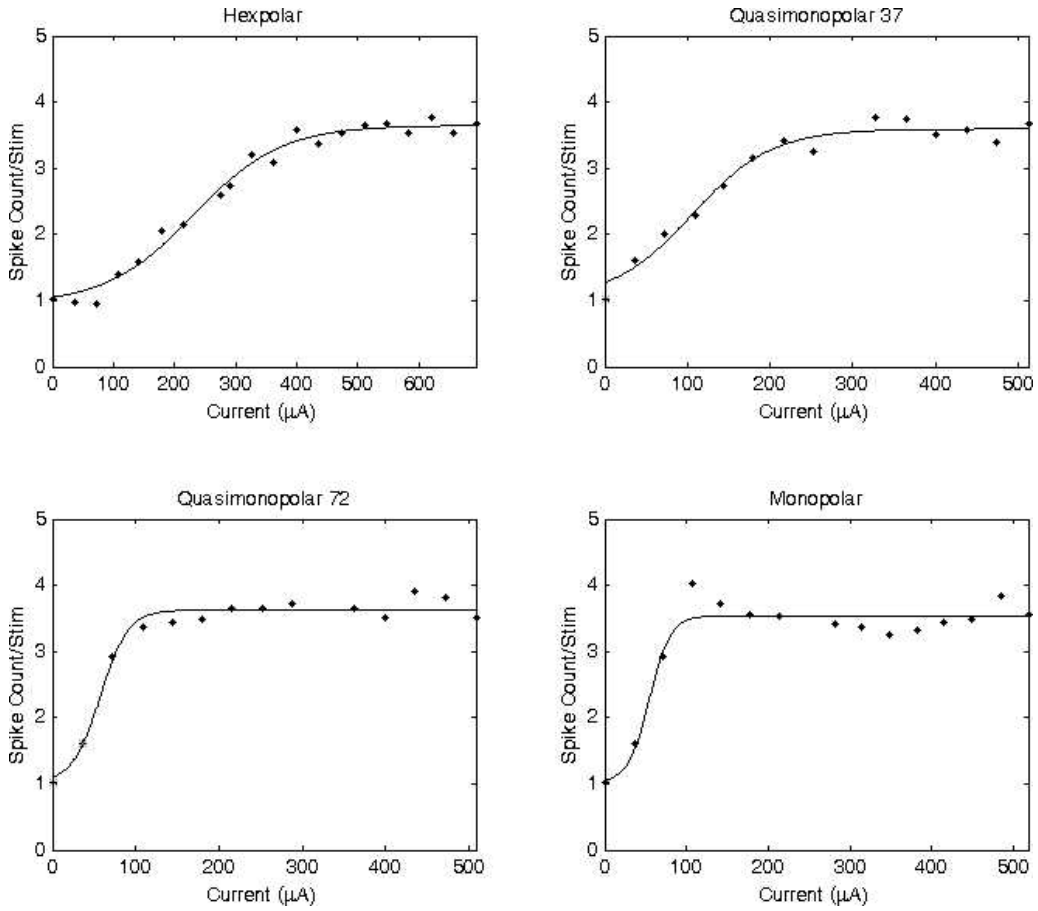

FIGURE 5. Sigmoid fits of the increase in single unit spiking activity as a consequence of an increase in current injection.

constant 400 μA for 400 μs via the retinal array. All cortical activity was monitored and recorded using a RZ2 TDT multichannel recording system (Tucker Davis Technologies, Inc., Alachua, FL), the single ball electrode was connected to a AM-Systems amplifier (AM-Systems, Sequim, WA), while all multielectrode arrays (MEA) were connected to the RZ2 through a PZ2 pre-amp unit by the same manufacturer. The stimulating electrodes chosen for mapping were those most efficacious at eliciting a response, usually in closest proximity to the area centralis and surrounded by a ring of guard electrodes. The area of maximum cortical response was identified as the area with the highest evoked cortical surface potential measured over an average of 100 stimuli. Once the area of maximum activity was identified, a further mapping was performed using a fine ball point electrode in 1 mm steps. Upon accurate identification of the most appropriate cortical site, a 96-channel (10 × 10 channels with 4 corner electrodes disabled, 5 × 5 mm, 1.5 mm pitch) recording-electrode Utah array (Blackrock Microsystems, Salt Lake City, UT) was inserted pneumatically.

The stimulating electrode array was connected through a PXI system (National Instruments Corporation, Austin, TX) to a constant-current stimulator developed in house. The isolated PXI chassis (PXI-1000B) system included a switch matrix (PXI-2532) to redirect the charge-balanced, constant current biphasic pulse,[41] generated by the stimulator, and a digital multimeter (DMM; PXI-4072) to acquire the resulting voltage waveform and determine values for electrode impedance as described by John et al.[42] The stimulator contained four constant-current stimulation chips described in Wong et al.[38]

Spike Detection

Data streaming from the 96-channel cortical array was recorded onto a custom built desktop PC. All data processing was performed offline using Matlab 2010 (MathWorks, Natick, MA). Data access to RZ2 TDT recording from Matlab was made available through the OpenDeveloper library provided by Tucker Davis Technologies, Inc. The current settings for the DACs are described in the Table. Each channel was downloaded, the artifacts in correspondence with the stimulus timestamps were removed using the method described by Heffer et al.,[43] whereby a 3 ms window around the artifact (1 ms before timestamp to 2 ms after timestamp) was replaced by linear intermediate voltage values. The signal then was band pass filtered between 300 and 5000 Hz using a fifth order Butterworth filter.

Spike threshold was calculated based on the 99% percentile signal voltage levels 100 ms preceding the stimulation:

$$T = k\frac{\sum_{i=-2.58\sigma}^{2.58\sigma} V(i)n(i)}{N} \quad (1)$$

where T is the threshold value, k is the threshold multiplier, V is the array of voltage values, n is the count of samples binned per voltage, σ is standard deviation, and N is the overall count of samples within the confidence interval (CI).

This threshold calculation eliminated the presence of random, high voltage electrical noise that was observed to be superimposed on the recording. The threshold multiplier was optimized for each animal to achieve an average response baseline of approximated one spike per second.

Epoch extraction began 3 ms after stimulus onset and lasted for 20 ms, to ensure that while all direct and network activation was included, that any stimulus artifact would be excluded. Spikes were detected by threshold crossing with a 1 ms window.

Sigmoid Fitting and Activation Thresholds

For each dataset, the sigmoidal relationship was observed in the average spike rate (%) with respect to the injected current (μA). The following equation was fitted to the trend:

$$y = base + \max\frac{\max}{1 + \exp\left(\frac{P50 - x}{rate}\right)} \quad (2)$$

where *base* is the baseline spiking rate, *max* is the maximum spike rate, *rate* is the gradient of the slope of the sigmoid, and *P*50 is the midpoint of the sigmoid's slope (Fig. 5).

The sigmoid was used to interpolate a current value at which the spike rate reaches that of half of maximum (P50), and this was used as an indication of variation in perceptual threshold.[36] Threshold values of P50 were calculated for hexapolar, monopolar, and quasimonopolar, and the results compared to determine the effect of combining hexapolar and monopolar stimulation on the resulting threshold level.

Conditional Probability Analysis

The first step of the analysis consisted of using the sigmoids fitted from the threshold analysis to identify the cortical site with the lowest P50 value across the retinal array for each stimulation configuration. This site will be referred to for simplicity as the best cortical electrode (BCE).

Using the data processed for the threshold analysis, the first 20 ms after artifact was observed for each recording and split into 5 ms windows. A binary representation of the 20 ms was made by generating an array of four values (one for each 5 ms window), with a 1 indicating the presence of a spike in that interval and a 0 indicating that no spikes were detected.

The principal aim of this analysis was the investigation of the spatial activation pattern following different stimulus configurations by means of measuring the cortical activation. As a consequence, only the 5 ms window from 2 ms poststimulus onset to 7 ms poststimulus onset was analyzed, as spikes detected within this phase are attributed to direct retinal ganglion cell activation.[44] This allowed us to focus the analysis on the shape of the stimulating field.

For the BCE, the probability of a spike occurring in the given interval P(BCE) was calculated by summing the values across all epochs and divided by the total number of repetitions of a single current setting. The result was a number between 0 and 1, where 0 indicated no spikes were recorded across any of the repeats for the observed current at the BCE, 0.1 indicated a presence of a spike in 10% of the repeats, and so on up to 1, indicating that a spike was detected in 100% of the repeats. For all other cortical electrodes ($E1_x$), the probability of a spike occurring simultaneously at the observed electrode and at the BCE [$P(E1_x \cap BCE)$] was calculated by counting the number of repetitions that concurrently reported a spike detected during the first window, on both the observed electrode and the BCE. Finally, the probability of a spike occurring at a given cortical site $E1_x$ given that it also occurred at the BCE [$P(E1_x|BCE)$] was calculated using Equation 3.

$$P(E1_x|BCE) = \frac{P(E1_x \cap BCE)}{P(BCE)} \quad (3)$$

where $P(E1_x \cap BCE)$ is the probability of a spike occurring at a cortical site $E1_x$ and BCE concurrently, and $P(BCE)$ is the probability of a spike occurring on the BCE.

The resulting probability map was observed for values of $P(BCE)$ approaching maximum, so for the first value where $P(BCE) > 90\%\ maxP(BCE)$. This value was selected because for lower values of $P(BCE)$, the stimulating current was not sufficient to maximize the BCE's response, and, therefore, the

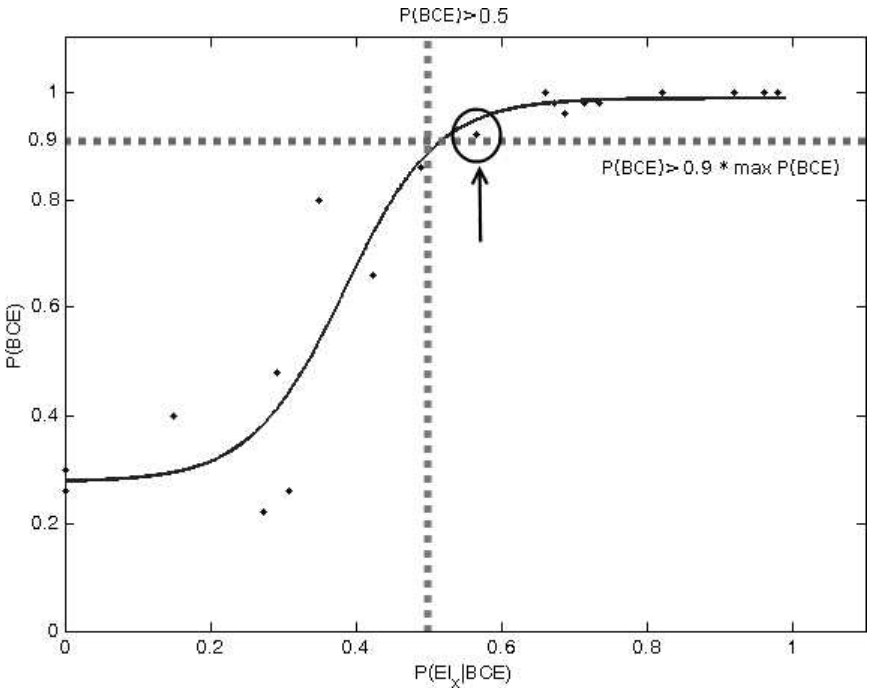

FIGURE 6. P(BCE) versus P(E1$_x$|BCE). The relation between the increase in the probability of a spike occurring on an observed electrode *X* given that it occurred on the BCE and a spike occurring on the BCE was used as a measure of cortical localization. The first value of P(E1$_x$|BCE) for P(BCE) > P90 (where P90 is the sigmoid value = 0.9 × max P[BCE]) is greater than 0.5 (highlighted with the *circle* and *arrow*), so the site is considered active. This is calculated for all cortical channels and allows the number of active sites to be calculated independently of their position with respect to the BCE.

current spread would not be maximized, making changes in charge containment more subtle and difficult to observe. On the other hand, if a larger value for *P(BCE)* had been chosen, *P(BCE)* would have remained at 1 (100% spiking rate), while the surrounding sites increased their *P(E1$_x$|BCE)*, and, thus, generating false results for activation localization.

The resulting value of *P(E1$_x$|BCE)* for *P(BCE)* > *P*90 was observed and if it was greater than an arbitrary threshold of 0.5, then the cortical site being analyzed was considered to be active and correlated to the BCE. The number of active channels was summed for each stimulating current value and for each stimulation strategy.

In this study, a sufficient charge was used for both hexapolar and monopolar stimulation to saturate the correlation between *P(E1$_x$|BCE)* and *P(BCE)* as illustrated in Figure 6. Once this charge level was observed, a value of P90 was chosen from the sigmoid and used to determine whether that specific cortical site was to be considered active or not. Hexapolar and monopolar data, therefore, were comparable because a similar probability of spikes occurred in the area of maximum cortical activity, implying that the corresponding retinal network was exposed to a similar charge.

Computational Simulations

To compare the extent of electric field penetration into the retina under various quasimonopolar and monopolar stimulation modes, we implemented a 3D computational finite-element model of electric field distribution in a single hex electrode configuration (Fig. 7). The relevant formulae are described in Equations 4 to 6.

$$\nabla.(-\sigma\nabla V) = 0 \quad (4)$$

$$\mathrm{E} = -\nabla V \quad (5)$$

$$\mathrm{J} = -\sigma\mathrm{E} \quad (6)$$

where *V* is the electric potential, *J* is the current density vector, σ is the electrical conductivity, and *E* is the electric field vector. A single hex electrode arrangement was implemented using COMSOL Multiphysics finite-element software 3-1 (COMSOL AB, Zurich, Switzerland), a disc electrode of 380 μm diameter, and center to center spacing of 1 mm.

RESULTS

During the course of the experiments, five animals were observed, recordings were made in response to stimulation from a total of 56 stimulating electrodes across all animals. Stimulation of electrodes positioned further from the area centralis did not always yield a sufficient response in V1 for subsequent analysis. Of these, 31 (55%) presented sufficient cortical response to allow for a sigmoid to be fitted and, consequently, to contribute to the results for activation threshold. The nature of the spatial localization allowed recordings to be used even if a clear sigmoid could not be fit, as long as there was activity across all of the stimulation strategies, resulting in 42 (75%) of the recording contributing to the data presented.

Computational Simulations

A finite element computation model was developed to understand better the orientation and containment of charge during quasimonopolar stimulation. A quasimonopolar stimulation was modeled by applying varying hexapolar and monopolar components to the stimulation electrode, and a user-specified fraction Q of this current was returned via a monopolar ground return electrode, located 2 mm above the plane of the hex electrode (Fig. 7). Conductivity σ of the

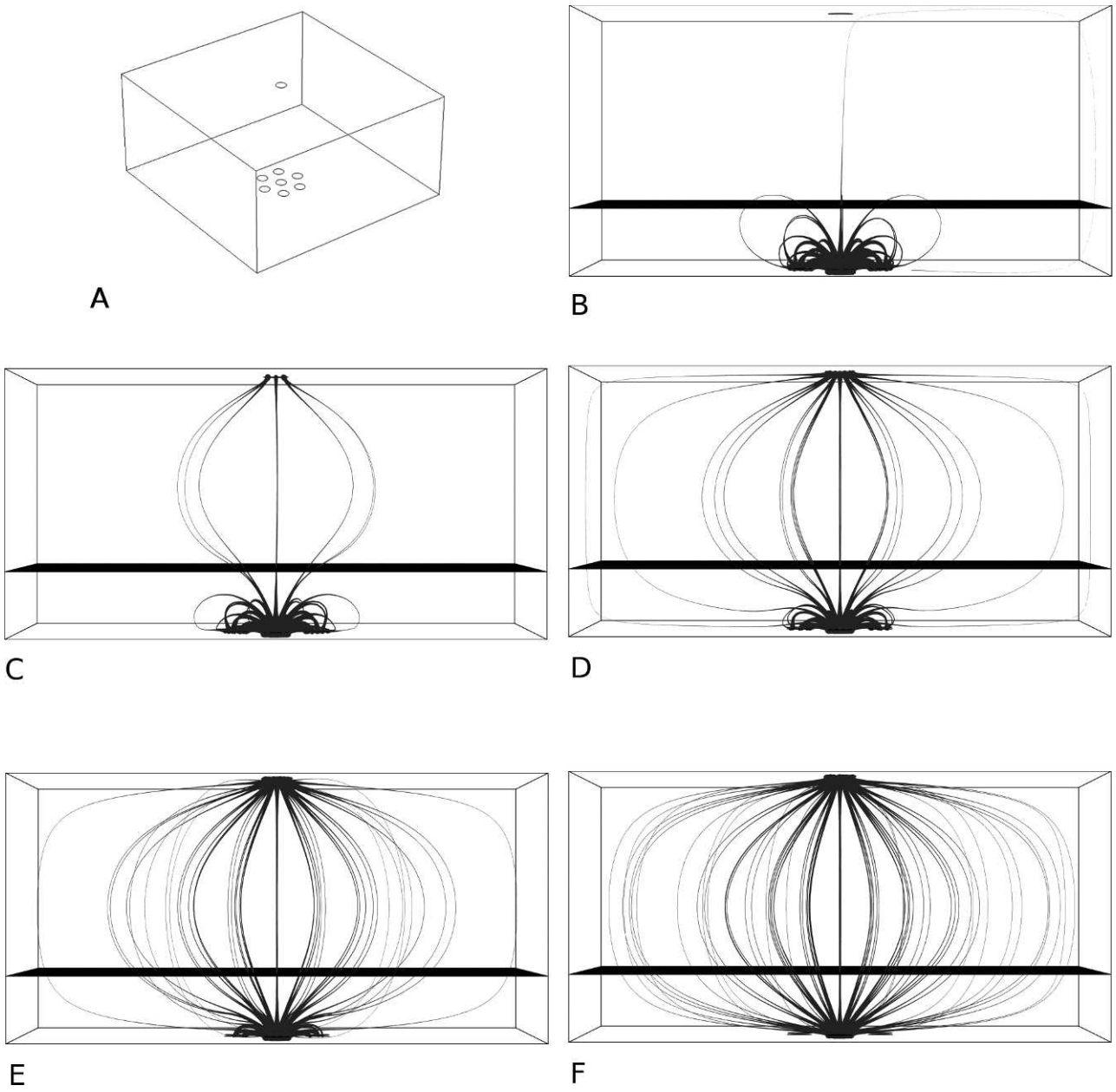

FIGURE 7. Simulations of quasimonopolar stimulation. (**A**) Illustrates an isometric view of the model with the stimulating electrode surrounded by a set of hexagonal return electrodes on the inferior plane, and the distant monopolar return located on the superior plane. (**B**–**F**) The current density streamlines for various stimulus modes. In each of these panels, the retinal target cell layer is shown as a horizontal plane offset from the lower boundary, with stimulating electrodes on the lower boundary and quasimonopolar return on the upper boundary. (**B**) A 300 μA pure hexapolar stimulus. Quasimonopolar stimulus with 200 μA hexapolar and 37 μA monopolar component (**C**), 100 μA hexapolar and 72 μA monopolar component (**D**), 50 μA hexapolar and 108 μA monopolar component (**E**), and 130 μA pure monopolar stimulation (**F**).

volume was set to 1 S/m, similar to that of physiological saline.

Activation Thresholds

During offline processing, the cortical responses to quasimonopolar stimulation were grouped by the amount of monopolar current being injected into the stimulating electrode. The monopolar and hexapolar currents then were summed into the total quasimonopolar current. For each monopolar current setting, the monopolar current was fixed and the hexapolar increased. A sigmoid then was fitted to overall quasimonopolar current and the P50 value extracted.

The output resolution of the stimulator allowed for increments of 40 μA (approximately 18 nC). The mean P50 value for each monopolar component was averaged for all recordings, and the results presented in Figure 8 illustrate the effect of increasing the subthreshold monopolar component to a pure hexapolar stimulation.

A monopolar contribution of zero resulted in only the hexapolar stimulation occurring. In agreement with the literature,[36] the values for threshold were 145 ± 13 (SE) nC. The addition of 19 nC of monopolar charge resulted in an

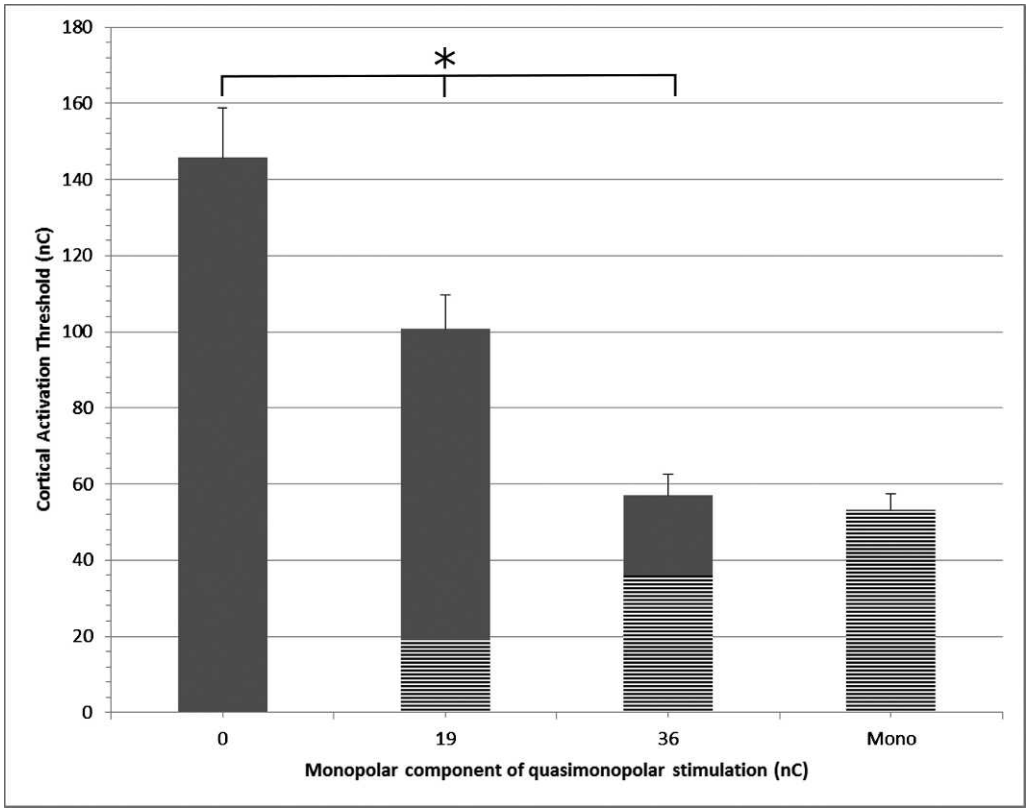

FIGURE 8. The effect on overall quasimonopolar threshold of increasing the stimulus monopolar component. With the increase of the monopolar component, there is a clear drop in threshold, as long as the monopolar component remains subthreshold. The *bar fills* indicate the ratio of monopolar (*hatched*) and hexapolar (*solid*) components of the quasimonopolar stimulus. $^*P > 0.05$ (*t*-test, $n = 5$ eyes, 31 stimulating electrodes). *Error bars* indicate standard error.

overall drop in the quasimonopolar threshold to 100 ± 8.9 (SE) nC (Fig. 9). Further increasing the monopolar charge to 36 nC resulted in a further reduction in threshold to 56.9 ± 5.7 (SE) nC. The activation threshold of pure monopolar stimulation was calculated as 53.2 ± 4 (SE) nC. Higher current values for the monopolar component of the quasimonopolar stimulus would exceed the monopolar threshold, and always result in cortical activation, and, thus, making it impossible for a P50 value to be determined.

Stimulation Localization

Conditional probability analysis was used to determine $P(E1_x|BCE)$, or the probability of a spike being detected at an observed cortical site, given that a spike had occurred on the BCE. The probability map then was observed for a current value such that $P(BCE) > P90$, and the number of channels with $P(E1_x|BCE) > 0.5$ counted (Fig. 10). The activity recorded in response to stimulation was grouped based on the monopolar component of the quasimonopolar stimulus (pure hexapolar or 0 nC, 19 nC, 36 nC, 54 nC, 71 nC, and pure monopolar). The final cortical activation map was expressed as a fraction to the number of responsive monopolar sites to eliminate the variability associated with the electrode placement, particular in close proximity to the fovea. The monopolar stimulation was chosen as the model predicted that pure monopolar stimulation yielded the widest retinal spread of activation.

In accordance with the mathematical modeling, when there was no monopolar component to the quasimonopolar stimulus (pure hexapolar), the resulting number of active cortical sites was 61.8% ± 5.5% (SE) of the sites activated by monopolar stimulation done. Increasing the monopolar component had little effect for 19 and 36 nC of monopolar charge, resulting in 66.4% ± 7.2% (SE) and 66.1% ± 5.5% (SE) of active sites relative to monopolar, and showing no statistical difference between the three for $P < 0.05$. A significant ($P > 0.05$) increase in activation was found when further increasing the monopolar component to 54 nC and 71 nC, with 86.4% ± 9.2% (SE) and 104% ± 7.4% (SE), respectively. No statistical significance in activation was found between the quasimonopolar stimulation using 71 nC of monopolar component and the pure monopolar stimulation (Fig. 11).

DISCUSSION

Cortical Thresholds

Results for monopolar suprachoroidal activation threshold of 53.2 ± 4 nC equates to a mean charge density of 46.9 ± 3.5 μC cm^{-2} using a 380 μm diameter electrode.

This value is comparable to the findings of Sakaguchi et al. (42 μC cm^{-2}) using a 500 μs phase and a 100 μm electrode[45]; Nakauchi et al.[46] (56 μC cm^{-2}), with a 180 μm electrode and 500 μs phase time; and Zhou et al. (48.64 μC cm^{-2}) using a 1 ms phase time and a 300 μm electrode.[23]

Monopolar and hexapolar (128.5 ± 11.4 μC cm^{-2}) results are within the range of studies by Wong et al.[31] (184 μC cm^{-2} for hexapolar and 63 μC cm^{-2} for monopolar) and Cicione et al.[36] (140 ± 66 μC cm^{-2} for hexapolar and 64 ± 36 μC cm^{-2}

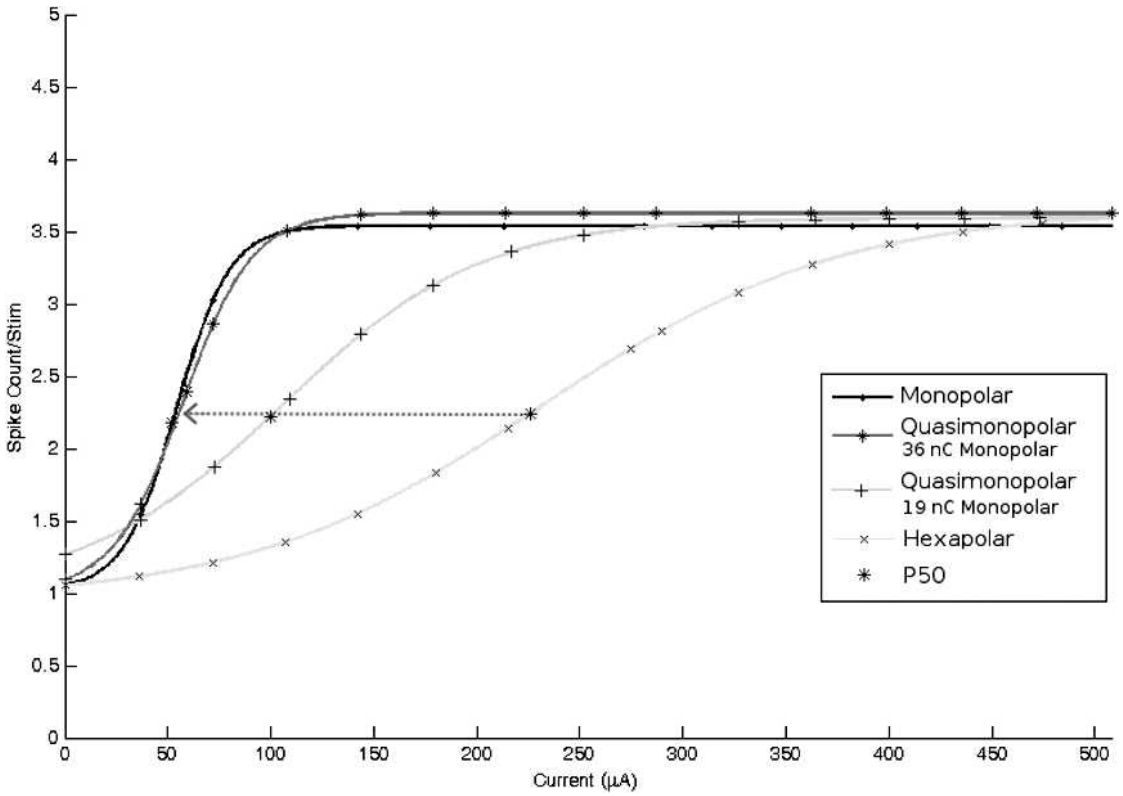

FIGURE 9. Shift in P50. The sigmoidal relation between injected current and cortical responses is illustrated. The P50 point on the sigmoids shifts (highlighted by the *arrow*) left as a consequence of a drop in activation threshold when comparing hexapolar (*highest*) to quasimonopolar and monopolar (*lowest*).

for monopolar) using 500 μs phase time and 600 μm diameter electrodes.

Variability exists between these studies, introduced by factors, such as interelectrode distance, electrode-tissue interface, and different fabrication techniques, which result in significantly different surface topography and, thus, differing effective electrode surface areas. However, in all studies that have compared monopolar and hexapolar stimulation, three times the charge density of monopolar is required to elicit a response using hexapolar stimuli. This is confirmed further by the mathematical model (Fig. 7) and studies by Joarder et al.[35]

Threshold difference likely arises from the high impedance nature of the choroid and retinal pigment epithelium[47,48]: monopolar stimulation, with a remote return electrode, is more likely to produce transretinal currents that stimulate the remaining retinal cells, unlike hexapolar stimulation, where a large amount of current shunts from the stimulating electrodes to the return electrodes without affecting the target cells.

By using a quasimonopolar configuration, the threshold can be lowered significantly with each increase in the monopolar component of the stimulation: 18.5 nC monopolar component reduced the threshold by 45 nC, and further increasing the monopolar component by 18 to 36 nC results in a further decrease in the threshold of 43.2 nC. It is interesting to note that for an equal increase of the monopolar component, there is an equal decrease in the overall quasimonopolar threshold. Moreover, the decrease in threshold equates to approximately three times the increase in monopolar component, thus confirming monopolar stimulation to be three times as effective as hexapolar in stimulating a target tissue from the suprachoroidal space in the normally sighted feline, but also indicating that for a hexapolar-injected current, only approximately a third of the current actively contributed to the stimulation in the geometry studied.

Monopolar stimulation from the suprachoroidal space is the current steering strategy that most directly traverses the retinal tissue, thus producing the lowest activation thresholds. When stimulating using a quasimonopolar stimulus with a subthreshold monopolar component, the hexapolar field will stimulate the network to the point of activation threshold; however, less hexapolar current will be required as the monopolar component will superimpose upon the hexapolar and cause a decrease in the level of activation threshold. Once the monopolar component exceeds the monopolar threshold, it is sufficient to activate the retinal network, and activation threshold is achieved entirely through the monopolar component. As a result, for quasimonopolar stimulations with a monopolar component at threshold, the overall activation threshold is optimal and no further benefit to activation threshold is gained by further increasing the monopolar component.

Cortical Localization

Studies of cochlear implants have shown that spatial distribution in the auditory cortex is affected by return configurations of the stimulating device.[49,50]

Wong et al. compared the cortical activation of hexapolar, bipolar, and tripolar current steering techniques, and concluded that hexapolar stimulation was more effective because of the smaller area of cortical activation.[31] Comparing hexapolar to monopolar, however, proved more difficult as one must ensure that the charge stimulating the surviving retinal cells is

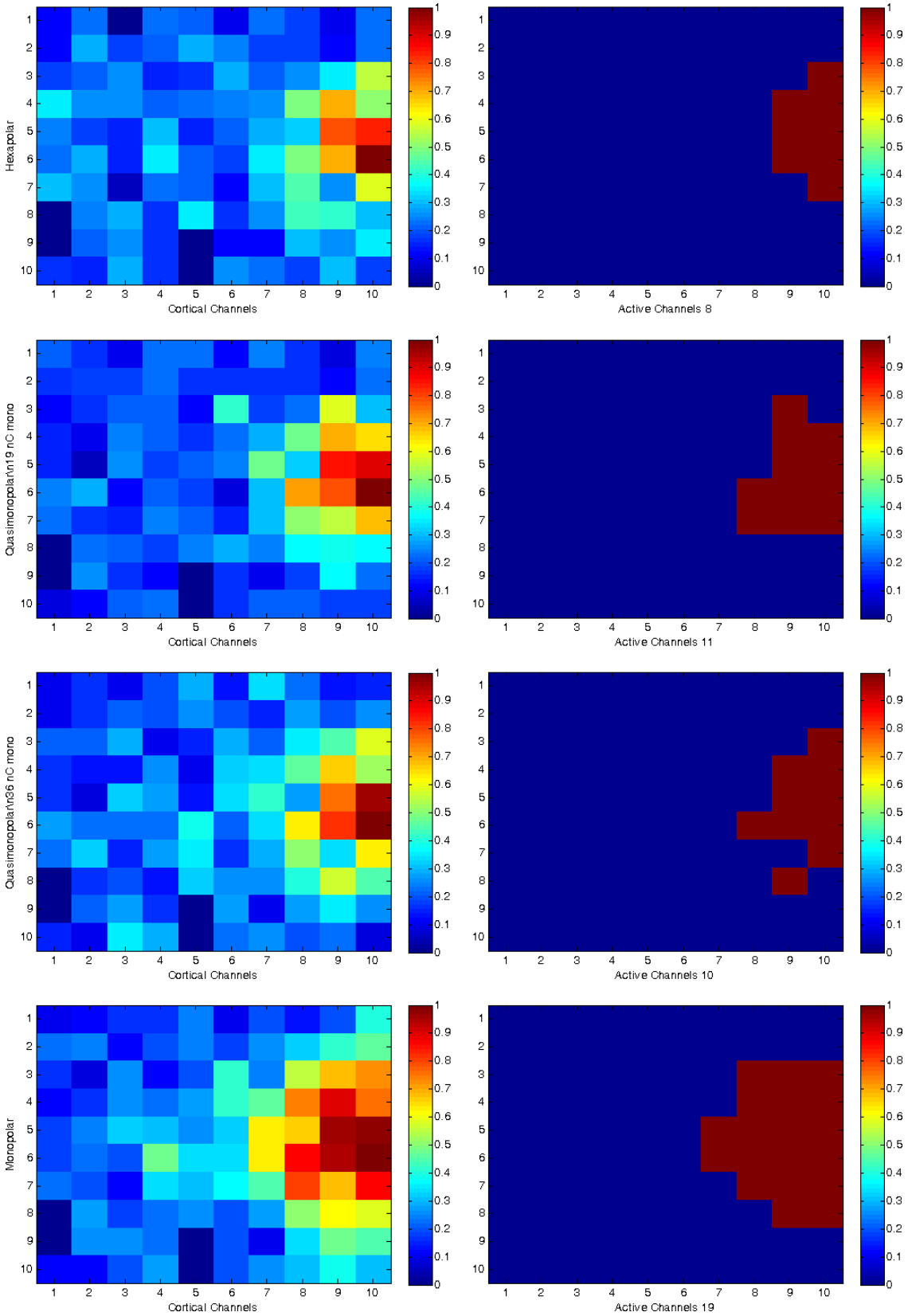

Figure 10. Example of conditional probability analysis. The probability map is illustrated on the *left* where $P(E1_x|BCE)$ is calculated for each cortical site. $P(E1_x|BCE)$ indicating the probability of a spike occurring at a specific site given that a spike was detected at the BCE. An example of hexapolar and monopolar strategies and two values of quasimonopolar strategy were observed for $P(BCE)$ and the results plotted. On the *right column* the binary representation of the active channels can be observed where $P(E1_x|BCE) > 0.5$. The overall number of active channels is also indicated.

Investigative Ophthalmology & Visual Science

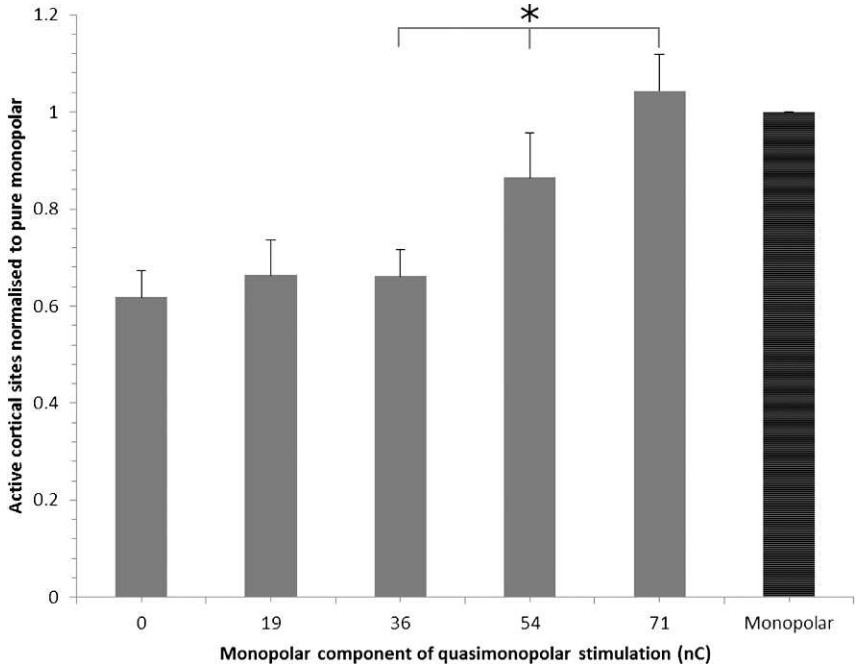

FIGURE 11. Effect of increasing the monopolar component on the overall localization of the quasimonopolar stimulus. Increasing the monopolar component below the monopolar threshold has no significant effect on focused activation. As the monopolar component approaches and exceeds threshold, activation focus tends to decrease and approximate that of pure monopolar stimulation (*hatched*). $^*P > 0.05$ (*t*-test, $n = 5$ eyes, 42 stimulating electrodes).

equal across different stimulating techniques to derive conclusions from cortical containment.

Previous studies also have indicated a correlation between retinal recruitment and cortical activation localization.[40] Recently, however, there has been evidence that the correlation does not always correspond to an equivalent increase in cortical localization.[36] This may be due to the complex mapping that exists between the retina and cortex, which does not imply that a circular increase in the area of retinal recruitment will correspond to a circular increase in the activity observed in the visual cortex. For this reason we developed an innovative method for analyzing spikes recorded in the primary visual cortex by using conditional probability to express correlation between different areas of V1 without requiring that the areas of activity be adjacent of geometrically similar to what observed in the retina.

For each cortical site, there is a correlation between $P(E1_x|BCE)$ and $P(BCE)$ as illustrated in Figure 6. The sigmoidal relation between $P(El_x|BCE)$ and $P(BCE)$ is dependent on the proximity of a given cortical site to the BCE.

The results illustrated in Figure 11 indicate that hexapolar stimulation is more effective at containing charge when compared to monopolar stimulation. These results are in agreement with the findings of the mathematical modeling of retinal stimulation[51,52] and also have been demonstrated in studies of cochlear implants[33] where tripolar stimulation was found to activate a smaller percentage of sites in the inferior colliculus. Although it is reasonable to assume that charge containment of a single stimulus actually results in an increase of perceptual acuity,[33,36] retinal localization becomes vitally important when implementing concurrent stimulations. This practice is uncommon in cochlear implants, as the summation of the electrical fields becomes extremely complex[53]; however, with the number of retinal electrodes increasing rapidly, the likelihood of sequential stimulation of single electrodes in series becomes less likely.

Quasimonopolar stimulation results in a combination of the spatial containment of its two component stimulations, and is influenced greatly by the monopolar component used. As for the threshold results, there appears to be a distinction between sub- and peri-/suprathreshold charges for the monopolar component of the stimulus. Subthreshold monopolar stimulations are insufficient to elicit a retinal (and, thus, cortical) response, and, therefore, the observed cortical activity is purely a consequence of the hexapolar stimulation, as there is no statistical difference between the active cortical sites for quasimonopolar with monopolar component with charges equal to 0, 18.5, and 36.5 nC. The effects of the monopolar component become apparent when its charge reaches monopolar threshold level (53 ± 4 nC). The cortical containment, therefore, is no longer a consequence purely of the hexapolar stimulation, but the monopolar component becomes the primary cause of retinal recruitment and, therefore, causes a significant increase in the active sites: by increasing the charge of the monopolar component of the quasimonopolar stimulation from 36 to 53.5 nC, the result is an increase of 20% of the cortical sites found to be active. Further increasing the monopolar component's charge to 71 nC results in an almost identical increase of 17% of active cortical sites.

Optimal Stimulation

Figure 12 summarizes the effect of monopolar contributions to quasimonopolar stimulation for thresholds and localization. These results indicated that the greater the monopolar contribution, the lower the overall threshold of the stimulation until pure monopolar threshold is reached. The requirement to contain the stimulating field, to achieve a focused stimulation warrant a subthreshold monopolar element, with most, if not all, advantages lost as soon as the monopolar threshold is exceeded. The optimal quasimonopolar stimulation for a suprachoroidal retinal prosthesis is one where the monopolar

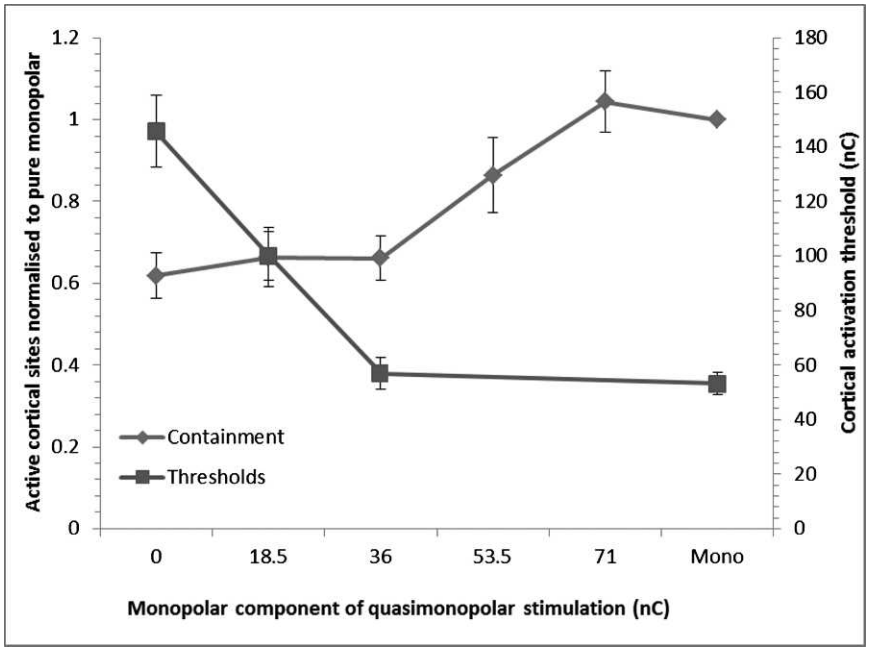

FIGURE 12. Overlap of the effects on thresholds and spatial localization of increasing the monopolar component of a quasimonopolar stimulation. *Error bars* indicate SE, $n = 5$.

element is as close to a monopolar neural threshold (not the P50 value used in this analysis), while remaining below that threshold. This results in a stimulation that provides a 30% improvement in spatial activation when compared to pure monopolar at threshold, and a reduction in excess of 60% of the required current to achieve activation threshold when compared to pure hexapolar stimulation. The improvement in localization is likely to equate to an improvement in the focus of the perceived phosphene.

The use of a monopolar component affect cross-talk between electrodes even with subthreshold stimuli,[33] however, by using a subthreshold monopolar component, cross-talk can be minimized, and phosphene modulation achieved using the more charge-containing hexapolar return configuration.

CONCLUSIONS

In our study we have proposed a novel technique for current steering in the suprachoroidal space. By concurrently stimulating with hexapolar and monopolar configurations, we obtained a quasimonopolar stimulus incorporating the best features of both stimulation strategies. In vivo results confirmed the prediction of the mathematical model, with the formation of two distinct and superimposed electrical fields. This led us to identifying a subthreshold monopolar component as being the optimal stimulus configuration for quasimonopolar. This technique could provide focal stimulation at a level comparable to hexapolar stimulation, but with a stimulus current much lower than hexapolar configuration, and approximating those of monopolar configuration.

Acknowledgments

The authors thank Phil Byrnes-Preston for his patient assistance; as well as Veronika Tatarinoff, Wenqi Huang, Adrian Bradd, Amgad Habib, and Richard Vickery for their help and support in in vivo preparation; Calvin Eiber for technical assistance and development of the stimulating and recording systems; and Brandon Bosse, Marc-Patrick Zapf, Jin Yu, and Cherry Ho for their continuous help.

Supported by the Australian Research Council (ARC) through its Special Research Initiative (SRI) in Bionic Vision Science and Technology Grant to Bionic Vision Australia (BVA).

Disclosure: **P.B. Matteucci**, None; **S.C. Chen**, None; **D. Tsai**, None; **C.W.D. Dodds**, None; **S. Dokos**, None; **J.W. Morley**, None; **N.H. Lovell**, None; **G.J. Suaning**, P

References

1. Liberson WT, HolmQuest HJ, Scot D, Dow M. Functional electrotherapy: stimulation of the peroneal nerve synchronized with the swing phase of the gait of hemiplegic patients. *Arch Phys Med Rehabil*. 1961;42:101–105.
2. Hopps JA, Bigelow WG. Electrical treatment of cardiac arrest: a cardiac stimulator-defibrillator. *Surgery*. 1954;36:833–849.
3. Clark GM, Tong YC, Black R, Forster IC, Patrick JF, Dewhurst DJ. A multiple electrode cochlear implant. *J Laryngol Otol*. 1977;91:935–945.
4. LeRoy C. Ou l'on rend compte de quelques tentatives que l'on a faites pour guérir plusieurs maladies par l'électricité. *Memoire Math Phys*. 1755;60.
5. Troyk P, Bak M, Berg J, et al. A model for intracortical visual prosthesis research. *Artif Organs*. 2003;27:1005–1015.
6. Normann RA, Maynard EM, Rousche PJ, Warren DJ. A neural interface for a cortical vision prosthesis. *Vision Res*. 1999;39:2577–2587.
7. Dobelle WH, Mladejovsky MG. Phosphenes produced by electrical stimulation of human occipital cortex, and their application to the development of a prosthesis for the blind. *J Physiol*. 1974;243:553–576.
8. Brindley GS, Lewin WS. The visual sensations produced by electrical stimulation of the medial occipital cortex. *J Physiol*. 1968;194:54–55P.
9. Brindley GS, Lewin WS. The sensations produced by electrical stimulation of the visual cortex. *J Physiol*. 1968;196:479–493.

10. Veraart C, Raftopoulos C, Mortimer JT, et al. Visual sensations produced by optic nerve stimulation using an implanted self-sizing spiral cuff electrode. *Brain Res*. 1998;813:181–186.
11. Duret F, Brelen ME, Lambert V, Gerard B, Delbeke J, Veraart C. Object localization, discrimination, and grasping with the optic nerve visual prosthesis. *Restor Neurol Neurosci*. 2006; 24:31–40.
12. Zrenner E. The subretinal implant: can microphotodiode arrays replace degenerated retinal photoreceptors to restore vision? *Ophthalmologica*. 2002;216(Suppl 1):8–20, discussion 52–53.
13. Yanai D, Weiland JD, Mahadevappa M, Greenberg RJ, Fine I, Humayun MS. Visual performance using a retinal prosthesis in three subjects with retinitis pigmentosa. *Am J Ophthalmol*. 2007;143:820–827.
14. Shire DB, Kelly SK, Chen J, et al. Development and implantation of a minimally invasive wireless subretinal neurostimulator. *IEEE Trans Biomed Eng*. 2009;56:2502–2511.
15. Siu TL, Morley JW. In vivo evaluation of an episcleral multielectrode array for stimulation of the retina with reduced retinal ganglion cell mass. *J Clin Neurosci*. 2008; 15:552–558.
16. Mokwa W, Goertz M, Koch C, Krisch I, Trieu HK, Walter P. Intraocular epiretinal prosthesis to restore vision in blind humans. *Conf Proc IEEE Eng Med Biol Soc*. 2008;2008:5790–5793.
17. Humayun MS, Prince M, de Juan E Jr, et al. Morphometric analysis of the extramacular retina from postmortem eyes with retinitis pigmentosa. *Invest Ophthalmol Vis Sci*. 1999;40:143–148.
18. Eckmiller R. Learning retina implants with epiretinal contacts. *Ophthalmic Res*. 1997;29:281–289.
19. Fried SI, Jensen RJ. The response of retinal neurons to electrical stimulation: a summary of in vitro and in vivo animal studies. In: Dagnelie G, ed. *Visual Prosthetics: Physiology, Bioengineering, Rehabilitation*. New York, NY: Springer; 2011.
20. Majji AB, Humayun MS, Weiland JD, Suzuki S, D'Anna SA, de Juan E Jr. Long-term histological and electrophysiological results of an inactive epiretinal electrode array implantation in dogs. *Invest Ophthalmol Vis Sci*. 1999;40:2073–2081.
21. Gerding H, Benner FP, Taneri S. Experimental implantation of epiretinal retina implants (EPI-RET) with an IOL-type receiver unit. *J Neural Eng*. 2007;4:S38–S49.
22. Chen J, Doyle P, Cai C, et al. Surgical implantation of 1.5 generation retinal implant in minipig eyes. *Invest Ophthalmol Vis Sci*. 2010;51:3052.
23. Zhou JA, Woo SJ, Park SI, et al. A suprachoroidal electrical retinal stimulator design for long-term animal experiments and in vivo assessment of its feasibility and biocompatibility in rabbits. *J Biomed Biotechnol*. 2008;2008:547428.
24. Wong YT, Chen SC, Kerdraon YA, et al. Efficacy of suprachoroidal, bipolar, electrical stimulation in a vision prosthesis. *Conf Proc IEEE Eng Med Biol Soc*. 2008;2008:1789–1792.
25. Kanda H, Morimoto T, Fujikado T, Tano Y, Fukuda Y, Sawai H. Electrophysiological studies of the feasibility of suprachoroidal-transretinal stimulation for artificial vision in normal and RCS rats. *Invest Ophthalmol Vis Sci*. 2004;45:560–566.
26. Villalobos J, Allen PJ, McCombe MF, et al. Development of a surgical approach for a wide-view suprachoroidal retinal prosthesis: evaluation of implantation trauma. *Graefes Arch Clin Exp Ophthalmol*. 2012;250:399–407.
27. Yamauchi Y, Franco LM, Jackson DJ, et al. Comparison of electrically evoked cortical potential thresholds generated with subretinal or suprachoroidal placement of a microelectrode array in the rabbit. *J Neural Eng*. 2005;2:S48–S56.
28. Walter P, Szurman P, Vobig M, et al. Successful long-term implantation of electrically inactive epiretinal microelectrode arrays in rabbits. *Retina*. 1999;19:546–552.
29. Rizzo R, Joseph F, Wyatt J, Loewenstein J, Kelly S, Shire D. Perceptual efficacy of electrical stimulation of human retina with a microelectrode array during short-term surgical trials. *Invest Ophthalmol Vis Sci*. 2003;44:5362–5369.
30. Horsager A, Greenberg RJ, Fine I. Spatiotemporal interactions in retinal prosthesis subjects. *Invest Ophthalmol Vis Sci*. 2010; 51:1223–1233.
31. Wong YT, Chen SC, Seo JM, Morley JW, Lovell NH, Suaning GJ. Focal activation of the feline retina via a suprachoroidal electrode array. *Vision Res*. 2009;49:825–833.
32. van den Honert, C, Stypulkowski PH. Single fiber mapping of spatial excitation patterns in the electrically stimulated auditory nerve. *Hear Res*. 1987;29:195–206.
33. Middlebrooks JC, Snyder RL. Auditory prosthesis with a penetrating nerve array. *J Assoc Res Otolaryngol*. 2007;8: 258–279.
34. Jolly CN, Spelman FA, Clopton BM. Quadrupolar stimulation for cochlear prostheses: modeling and experimental data. *IEEE Trans Biomed Eng*. 1996;43:857–865.
35. Joarder SA, Abramian M, Suaning GJ, Lovell NH, Dokos S. A continuum model of retinal electrical stimulation. *J Neural Eng*. 2011;8:066006.
36. Cicione R, Shivdasani MN, Fallon JB, et al. Visual cortex responses to suprachoroidal electrical stimulation of the retina: effects of electrode return configuration. *J Neural Eng*. 2012;9:036009.
37. Dodds CWD, Schuettler M, Guenther T, Lovell NH, Suaning GJ. Advancements in electrode design and laser techniques for fabricating micro-electrode arrays as part of a retinal prosthesis. *Conf Proc IEEE Eng Med Biol Soc*. 2011;2011: 636–639.
38. Wong YT, Dommel N, Preston P, et al. Retinal neurostimulator for a multifocal vision prosthesis. *IEEE Trans Neural Syst Rehabil Eng*. 2007;15:425–434.
39. Rose TL, Robblee LS. Electrical stimulation with Pt electrodes. VIII. Electrochemically safe charge injection limits with 0.2 ms pulses. *IEEE Trans Biomed Eng*. 1990;37:1118–1120.
40. Tusa RJ, Palmer LA, Rosenquist AC. The retinotopic organization of area 17 (striate cortex) in the cat. *J Comp Neurol*. 1978;177:213–235.
41. Lilly JC, Hughes JR, Alvord EC Jr, Galkin TW. Brief, noninjurious electric waveform for stimulation of the brain. *Science*. 1955;121:468–469.
42. John SE, Shivdasani MN, Leuenberger J, et al. An automated system for rapid evaluation of high-density electrode arrays in neural prostheses. *J Neural Eng*. 2011;8:036011.
43. Heffer LF, Fallon JB. A novel stimulus artifact removal technique for high-rate electrical stimulation. *J Neurosci Methods*. 2008;170:277–284.
44. Freeman DK, Fried SI. Multiple components of ganglion cell desensitization in response to prosthetic stimulation. *J Neural Eng*. 2011;8:016008.
45. Sakaguchi H, Fujikado T, Fang X, et al. Transretinal electrical stimulation with a suprachoroidal multichannel electrode in rabbit eyes. *Jpn J Ophthalmol*. 2004;48:256–261.
46. Nakauchi K, Fujikado T, Kanda H, et al. Transretinal electrical stimulation by an intrascleral multichannel electrode array in rabbit eyes. *Graefes Arch Clin Exp Ophthalmol*. 2005;243: 169–174.
47. Miller SS, Steinberg RH. Active transport of ions across frog retinal pigment epithelium. *Exp Eye Res*. 1977;25:235–248.
48. Brindley GS. The passive electrical properties of the frog's retina, choroid and sclera for radial fields and currents. *J Physiol*. 1956;134:339–352.

49. Snyder RL, Middlebrooks JC, Bonham BH. Cochlear implant electrode configuration effects on activation threshold and tonotopic selectivity. *Hear Res*. 2008;235:23–38.
50. Bierer JA, Middlebrooks JC. Auditory cortical images of cochlear-implant stimuli: dependence on electrode configuration. *J Neurophysiol*. 2002;87:478–492.
51. Wilke RGH, Moghadam GK, Lovell NH, Suaning GJ, Dokos S. Electric crosstalk impairs spatial resolution of multi-electrode arrays in retinal implants. *J Neural Eng*. 2011;8:046016.
52. Lovell NH, Hallum LE, Chen SC, et al. Advances in retinal neuroprosthetics. In: Akay M, ed. *Handbook of Neural Engineering*. New York, NY: John Wiley & Sons, Inc.; 2006: 337–356.
53. Shepherd RK, Seligman PM. Cochlear Implants. In: Horck KW, Dhillon GS, eds. *Neuroprosthetics: Theory and Practice*. Singapore: World Scientific Publishing Co PTE LTD; 2004: 878–904.

Investigative Ophthalmology & Visual Science